

# VLBI STUDY OF WATER MASER EMISSION IN THE SEYFERT 2 GALAXY NGC 5793. I: IMAGING BLUESHIFTED EMISSION AND THE PARSEC-SCALE JET

YOSHIAKI HAGIWARA

*Max-Planck-Institut für Radioastronomie, Auf dem Hügel 69, D-53121, Bonn, Germany*

`hagi@mpifr-bonn.mpg.de`

PHILIP J. DIAMOND

*Jodrell Bank Observatory, University of Manchester, Macclesfield Cheshire SK 11 9DL, UK*

and

NAOMASA NAKAI AND RYOHEI KAWABE

*Nobeyama Radio Observatory, Minamimaki, Minamisaku, Nagano, 384-1305, Japan*

## ABSTRACT

We present the first result of VLBI observations of the blueshifted water maser emission from the type 2 Seyfert galaxy NGC 5793, which we combine with new and previous VLBI observations of continuum emission at 1.7, 5.0, 8.4, 15, and 22 GHz. Maser emission was detected earlier in single-dish observations and found to have both red- and blueshifted features relative to the systemic velocity. We could image only the blueshifted emission, which is located 3.6 pc southwest of the 22 GHz continuum peak. The blueshifted emission was found to originate in two clusters that are separated by 0.7 milliarcsecond (0.16 pc). No compact continuum emission was found within 3.6 pc of the maser spot. A compact continuum source showing a marginally inverted spectrum between 1.7 and 5.0 GHz was found 4.2 pc southwest of the maser position. The spectral turnover might be due to synchrotron self-absorption caused by a shock in the jet owing to collision with dense gas, or it might be due to free-free absorption in an ionized screen possibly the inner part of a disk, foreground to the jet.

The water maser may be part of a maser disk. If so, it would be rotating in the opposite sense to the highly inclined galactic disk observed in CO emission. We estimate a binding mass within 1 pc of the presumed nucleus to be on the order of  $10^7 M_{\odot}$ . Alternatively, the maser emission could result from the amplification

of a radio jet by foreground circumnuclear molecular gas. In this case, the high blueshift of the maser emission might mean that the masing region is moving outward away from the molecular gas surrounding an active nucleus.

*Subject headings:* water masers: extragalactic, jet—AGN: NGC 5793

## 1. INTRODUCTION

VLBI observations of water megamasers on (sub-)pc scales in active galaxies have proven to be a basic tool for investigating the central regions of active galactic nuclei (AGN). The most impressive result from this kind of research was the discovery of a thin, nearly edge-on rotating disk around a super massive black hole at the center of NGC 4258 (Miyoshi et al. 1995; Greenhill et al. 1995a). The VLBI observations revealed the size and the shape of the slightly-warped maser disk with a central radio jet outflowing perpendicularly to the disk plane (Herrnstein et al. 1998). VLBI imaging of the water megamasers in NGC 1068, NGC 4945 and the Circinus galaxy showed the possible existence of super massive objects at their nuclei similar to NGC 4258 (Greenhill et al. 1996; Greenhill & Gwinn 1997; Greenhill et al. 1997; Greenhill 2000). According to the most recent result, in the Seyfert 2 galaxy IC 2560, the barely resolved maser spots which constitute the systemic emission show a linear velocity gradient along the north-south elongation and are accompanied by continuum emission, probably suggesting a super massive black hole inside a rotating disk (Nakai et al. 1998; Ishihara et al. 2001). In the Seyfert 2 galaxy NGC 1068, in addition to the nuclear disk-maser, non-disk maser emission was found some 30 pc away along the jet from the radio nucleus, that might be the result of interaction between the jet and the interstellar gas (Gallimore et al. 1996). In the elliptical galaxy NGC 1052, the interpretation of non-disk masers was introduced to explain the water masers seen lying along the jet (Claussen et al. 1998). Water megamasers seem to fall into two categories: nuclear masers residing in a (sub-)parsec scale disk around an active nucleus and non-nuclear masers which are seen significantly further from the nucleus. The latter can also be classified into two types, that is, jet masers associated with radio jets and outflow masers – a wind component discovered in Circinus (Greenhill 2000). The study of non-disk maser emission is equally important for the investigation of the overall structure surrounding an active nucleus. In order to understand the megamaser phenomenon, and to deduce the general characteristics of the central parsecs of AGN, such as black hole masses and accretion rates, it is important to investigate as many megamasers as possible with VLBI imaging at milliarcsecond angular resolutions. So far, more than 20 galaxies are reported to contain megamasers (e.g., Braatz et al. 1997, Falcke et al. 2000). Most of them, however, show weak intensities, and some are

thus not observable with VLBI (Moran et al. 1999).

NGC 5793 is an edge-on disk galaxy, at a distance of 46 Mpc, with a compact nucleus seen in radio continuum emission (Gardner et al. 1992). Baan et al. (1998) classified the nucleus as being a Seyfert 2 from its optical emission. Hagiwara et al. (1997), using the Nobeyama 45-m telescope, first detected the water maser emission with highly Doppler-shifted satellite features, displaced by  $245 \text{ km s}^{-1}$  on either side of the systemic velocity ( $V_{\text{sys, LSR}} = 3442 \text{ km s}^{-1}$ ; Palumbo et al. 1983) of the galaxy. The total isotropic luminosity of the maser was estimated to be  $106 L_{\odot}$ . Fig. 1 shows a new spectrum of blueshifted maser features measured with the Parkes 64-m telescope. There may be a suggestion of features near the systemic velocity, which needs confirming. The highly redshifted features at  $V_{\text{LSR}} = 3677 \text{ km s}^{-1}$ , which were initially detected with the 45-m remain undetected since February 1996. From 1996 we began VLBI observations using the NRAO<sup>1</sup> VLBA and VLA, investigating the spatial distribution of the water maser emission and the relationship between the water megamasers and the nuclear radio activity of NGC 5793.

In this paper we describe the VLBA observations in Section 2, present new images of the water vapour maser line and continuum emission in the central parsecs of NGC 5793 in Section 3, and discuss the nature of the water maser in Section 4. We adopt a distance of 46 Mpc to NGC 5793, corresponding to a scale of 1 milliarcsecond (mas)  $\approx 0.23 \text{ pc}$ .

## 2. VLBA OBSERVATIONS AND DATA ANALYSIS

### 2.1. 22 GHz Observations

We observed the  $6_{16} - 5_{23}$  maser line at 22 GHz (rest frequency: 22.23508 GHz) toward NGC 5793 for 8 hours on 1998 May 10 using the VLBA and the phased VLA. The use of the VLA as the eleventh array element was critical to the observation because the peak flux density of the maser emission is known to be very weak ( $\sim 0.1 \text{ Jy}$ ). The data were recorded in left circular polarization with 2 bit sampling in four 8 MHz IF bands of 128 spectral channels each providing a velocity coverage of  $108 \text{ km s}^{-1}$ . The four IF bands were centered on  $V_{\text{LSR}} = 3190, 3442, 3551, \text{ and } 3667 \text{ km s}^{-1}$ . The observed velocity ranges are displayed in a single-dish spectrum in Fig. 1. The channel spacing in each band was  $0.83 \text{ km s}^{-1}$  before averaging. We observed in a phase-referencing mode, using a bright calibration source 1507–168 about 2 degrees away from NGC 5793. The total cycle time was two minutes; 1-minute scans on 1507–168 and NGC 5793 alternated. The total amount of time

---

<sup>1</sup> The National Radio Astronomy Observatory is a facility of the National Science Foundation operated under cooperative agreement by Associated Universities, Inc.

spent integrating on the target source was about 150 minutes. 4C 39.25 and 3C 345 were used for both bandpass and amplitude calibration. All the data were correlated in NRAO Socorro and calibrated and reduced with AIPS. The fringe-fit solutions (phase, rate, and delay) obtained from the calibrator were applied to the IFs containing both the line plus continuum emission. Five spectral channels were averaged together to  $4.2 \text{ km s}^{-1}$  to obtain reasonable sensitivities. The positions of the maser emission on the sky were determined by 2-D Gaussian fitting to the maps. To make a continuum map, we averaged all spectral channels in a line-emission-free IF, centered on  $3667 \text{ km s}^{-1}$ .

The continuum and line maps were both made from differently weighted data to get reasonable sensitivities, resulting in a synthesized beam size of  $2.8 \times 1.8 \text{ mas}$  for the continuum map, and  $1.8 \times 1.0 \text{ mas}$  for the line map. The rms noise levels are  $1.3 \text{ mJy beam}^{-1}$  for the continuum map produced from a single bandwidth of 8 MHz and  $4.3 \text{ mJy beam}^{-1}$  for the continuum-subtracted line map for each averaged channel. The continuum emission was subtracted only in the region close to C1(C).

## 2.2. Observations at 1.7, 8.4, and 15 GHz

The 1.7, 8.4, and 15 GHz continuum observations were made on 1999 October 10, using 8 elements of the VLBA. The VLBA stations Brewster (BR) and Saint Croix (SC) did not take part in the observations. The four 8 MHz IF bands with left circular polarization were recorded using 2 bit sampling across a total bandwidth of 32 MHz. We used the frequency agility of the VLBA to switch rapidly among the three frequencies to obtain better  $(u, v)$  coverages with optimal observing time. The observing frequencies were switched typically every 7–10 minutes between 8.4 and 15 GHz. The 1.7 GHz observation was inserted among the other two frequencies about every 40 minutes. The 8.4 and 15 GHz observations were made using the phase-referencing method, with the same calibrator as at 22 GHz. At 8.4 GHz a total cycle time of about 4 minutes was used for the calibrator and the galaxy; 3-minute scans on the calibrator and 1-minute scans for the target source were employed. At 15 GHz, 1-minute scans on the calibrator and the target source were alternated. The total integration time spent on the target source at each frequency ranged from 60 to 120 minutes. The correlation of all the data was performed at Socorro. The data were calibrated using standard AIPS software. The amplitude calibration was made with observations of 4C 39.25 and 3C 345. The centroid position of the 8.4 GHz continuum source was determined from the phase-referenced map. Finally, self-calibration was used on the data at 1.7 and 8.4 GHz to improve the sensitivity of images with DIFMAP.

The maps were made from uniformly weighted data and the resultant synthesized beam sizes are  $23 \times 3.7 \text{ mas}$  at 1.7 GHz,  $7.0 \times 2.7 \text{ mas}$  at 8.4 GHz, and  $2.9 \times 0.6 \text{ mas}$  at 15 GHz.

The rms noise levels are 0.86 mJy beam<sup>-1</sup> for the 1.7 GHz map, 0.35 mJy beam<sup>-1</sup> for the 8.4 GHz map, and 0.82 mJy beam<sup>-1</sup> for the 15 GHz map at total bandwidths of 32 MHz.

### 2.3. Analysis of Positional Errors

The positional errors ( $\Delta\theta$ ) in the VLBI images, dominated by statistical noise, were estimated from the synthesized beam size ( $\theta_b$ ) divided by the signal-to-noise ratios (SNR). When we estimate relative positional errors between line and continuum maps, they are approximately given by the the equation

$$\Delta\theta_{mc} \simeq \sqrt{\left(\frac{\theta_{bm}}{2SNR_m}\right)^2 + \left(\frac{\theta_{bc}}{2SNR_c}\right)^2},$$

where  $m$  and  $c$  represent maser and continuum emission images. Thus, the relative positional error between one of the maser lines at the  $V_{\text{LSR}} = 3194$  km s<sup>-1</sup> feature and the 22 GHz continuum peak C1(C) is  $\theta_{mc} \sim 0.22$  mas.

The common reference positions (0, 0) (continuum peak C1(C)) were determined at various frequencies by phase-referencing to the compact source, 1507–168. This same calibrator was used for all the observing epochs and there seemed to be neither structural nor positional changes between the two epochs, May 1998 and October 1999. The alignment of the reference positions between the 22 and 8.4 GHz continuum maps was determined from the phase-referenced maps. Assuming that the position error of the common reference source and any structural changes of the reference source between epochs are negligible, the relative positional error between 22 GHz ( $k$ ) and 8.4 GHz ( $x$ ) is estimated as the following,

$$\Delta\theta_{mcx} \simeq \sqrt{\left(\frac{\theta_{bm}}{2SNR_m}\right)^2 + \left(\frac{\theta_{bcx}}{2SNR_{cx}}\right)^2 + \left(\frac{\theta_{brk}}{2SNR_{rk}}\right)^2 + \left(\frac{\theta_{brx}}{2SNR_{rx}}\right)^2},$$

where  $c$  and  $r$  represent continuum images of a target source and a phase-reference source. In our analysis, the third and fourth term in the formula are negligible as SNR of reference calibrator images are better by on the order of 10 – 100 than those of masers or 22 and 8.4 GHz continuum images of NGC 5793. Consequently, the relative uncertainty of the maser position with respect to the reference point at 8.4 GHz in Fig. 3 is  $\sqrt{(\theta_{bm}/2SNR_m)^2 + (\theta_{bcx}/2SNR_{cx})^2} = \sqrt{(2/(2 \cdot 11))^2 + (7/(2 \cdot 22))^2} \sim 0.2$  mas. (The inserted values were adopted from the phase-referenced maps without self-calibration.)

### 3. RESULTS

#### 3.1. Continuum Emission

Fig. 2 and Fig. 3 show radio continuum images at 22 and 8.4 GHz, from which we can identify at least four continuum components C1(C), C2(E), C2(C) and C2(W). The naming of the components follows the convention used in Hagiwara et al. (2000). The 22 GHz peak is coincident with C1(C) in the 8.4 GHz map to an accuracy of 0.25 mas, as estimated in the previous section. The basic morphological structure is quite similar to those at 1.7 and 5.0 GHz given in Fig. 2 and Fig. 3 of the paper by Hagiwara et al. (2000), but at both 15 and 22 GHz only C1(C) is detected. Table 1 lists the Gaussian-fitted peak flux densities of the major compact continuum sources identified at the five frequencies, and Table 2 lists the spectral indices of each component. The flux density and spectral indices were obtained by convolving with the same beam size corresponding to that of the 1.7 GHz map in 1996 to avoid resolution effects. The poor  $(u, v)$  coverage for the 1.7 GHz observing session in Oct. 1999 resulted in relatively inaccurate component flux densities in comparison with those in Nov. 1996. Fig. 4 shows spectra from four major components imaged in Fig 3. C1(C) shows steep spectral indices  $\alpha < -0.70$  (using the convention that  $S_\nu \propto \nu^\alpha$ , where  $S_\nu$  is the flux density at frequency  $\nu$ ) from 1.7 GHz to 15 GHz but a flat index  $\alpha \simeq -0.02$  between 15 GHz and 22 GHz. C2(C) and C2(W) have similar spectra:  $\alpha = -0.88$  and  $-0.99$  between 5.0 and 8.4 GHz, and  $\alpha = -0.46$  and  $-0.72$  between 1.7 and 5.0 GHz. The compact component C2(E) that lies within the jet extension and shows an inverted spectrum  $\alpha \simeq +0.13$  between 1.7 GHz and 5.0 GHz. The continuum peak of C2(E) was not clearly seen at 1.7 GHz in both epochs, but was seen in a 1.4 GHz map obtained in Dec. 1996 (Pihlström et al. 2000).

#### 3.2. Water Maser Emission

We detected maser features that are blueshifted with respect to the systemic velocity of the galaxy with the VLBA. The maser features are seen in the averaged channels ranging from  $V_{\text{LSR}} = 3190 \text{ km s}^{-1} - 3210 \text{ km s}^{-1}$ . Inset into Fig. 5 is a blueshifted spectrum that shows the total flux density obtained from our VLBA observations. The spectrum appears to be a scaled-down version of the the single-dish spectrum, which suggests that about 50 % of the peak flux density is detected in VLBA observations. This might be explained by the intrinsic intensity variability of the water emission or by a loss of coherence during phase referencing (Carilli and Holdaway 1999) or, of course, by a combination of both. Given the total maser intensity ( $0.78 \text{ Jy km s}^{-1}$ ) estimated from the VLBA spectrum shown in the inset in Fig. 5, the isotropic luminosity of the blueshifted emission is  $38 L_\odot$ , which is comparable

to that of the redshifted emission ( $22 L_{\odot}$ ) in NGC 4258 (Nakai et al. 1995). Fig. 5 shows the spatial distribution of the water maser spots, where the position of each maser feature was determined by Gaussian fitting for each emission peak in the deconvolved images that was detected above  $4\sigma$  level. Our analysis showed that the detected maser emission is split into two clusters with a separation of  $\sim 0.7$  mas, or 0.16 pc, but there is no discernible velocity structure. Each maser clump, assuming a nominal size of 0.2 mas, yields a lower limit to the brightness temperature,  $T_b \sim 10^9$  K. The centroid position of the brightest maser feature centered at  $V_{\text{LSR}} = 3194$  km s $^{-1}$  is marked with a cross in Fig. 2 and Fig. 3 in which the continuum maps are superposed. No continuum emission was detected at the maser position at any of our observed frequencies. The maser spot is located 15.5 mas or 3.6 pc from the unresolved radio continuum peak C1(C) at 22 GHz, which is coincident with a reference point (0, 0) in the 8.4 GHz map in Fig. 3. From VLA-A observations with a beam size of  $130 \times 80$  mas ( $30 \times 18$  pc) in 1997 January, this blueshifted maser emission remained unresolved, and was coincident with the unresolved continuum peak C1(C), supporting our VLBA results in this paper. The peak of C2(E) at 8.4 GHz is about 18 mas, some 4 pc away from the maser spot, suggesting that the maser clusters are located nearly at the midpoint of the line joining C1(C) and C2(E).

We found no velocity features of the water maser corresponding to the velocities of the HI and OH absorptions, observed with the VLA by Gardner et al. (1986).

## 4. DISCUSSION

### 4.1. Location of the Nucleus

One might ask where the nucleus of NGC 5793 lies? In order to understand the kinematics of the nuclear region in the galaxy we need to address this question. Component C1(C) shows a flat-spectrum at higher frequencies, at which it is not resolved, suggesting that it might be the ‘true’ nucleus. On the other hand, the ‘true’ nucleus may lie in the continuum emission gap between C1(C) and C2(E) where the maser spots are located. This would mean that the radio continuum nucleus could be highly obscured by a screen of dense ionized gas. In some megamasers like NGC 1068 (Greenhill et al. 1996), the Circinus galaxy (Greenhill 2000), and possibly NGC 4945 (Greenhill et al. 1997), the existence of maser disks has been confirmed but continuum emission has not been detected in the vicinity of the water masers.

The measured surface brightness of C2(E) is at least  $3.2 \times 10^8$  K and could in principle be as high as the  $\sim 10^{10}$  K required for synchrotron self-absorption (Kellermann & Pauliny-Toth 1969). It is conceivable that component C2(E) was produced by a strong shock with the circum-

nuclear gas. A jet ejected from the nucleus could be bent and deflected near C2(E) and extend further out to component C2(W). Alternatively, component C2(E) could be free-free absorbed by dense ionized foreground gas. The spectral index of +0.13 between 1.7 and 5.0 GHz is not steep enough for free-free absorption, but as it is a lower limit, it is not inconsistent with such an hypothesis. If C2(E) is a free-free absorbed component, it could be the inner part of the disk/torus. However, at this stage we *conservatively* consider that the spectral turnover of C2(E) is due to synchrotron self-absorption caused by the collision of a jet from the central engine with a dense gas in the circumnuclear region.

There might be a change in flux density during the two observing sessions between Oct. 1999 at 1.7 GHz and Oct. 1997 at 5.0 GHz. If so, the determination of the spectral index of C2(E) is unreliable. However, the flux density of C2(E) for 1.7 GHz in Nov. 1996 is quite similar with that in Oct. 1999, hence it is less likely that there was significant flux density variation from 1996 to 1999 as for C2(E). In any case, there is no straightforward interpretation for the location of the 'true' core. For this reason it is impossible to decide at present whether the water emission in NGC 5793 is a nuclear or non-nuclear maser.

#### 4.2. *Origins of the Water Maser*

Interpretation of the geometry of the detected maser emission in NGC 5793 is not straightforward, because the blueshifted features are located between continuum peaks and the velocity fields do not show any systematic trends. However, we discuss two possibilities to explain the nature of the maser in the galaxy:

- 1 The water maser in NGC 5793 results from the amplification of a radio jet by the circumnuclear molecular gas foreground to the jet.
- 2 The maser lies in a compact molecular disk rotating around the galactic nucleus, like that in NGC 4258.

Support for the validity of the first model comes from the presence of molecular (OH) gas with a parsec-scale distribution seen in absorption against the continuum structure with the VLBA (Hagiwara et al. 2000). The brightness of a putative radio jet component may not be sufficient to be detected by VLBI in NGC 5793 at 22 GHz. The brightness temperature of any undetected 22 GHz continuum source near the maser spots is less than  $\sim 10^7$  K, assuming that the peak flux density is  $6.5 \text{ mJy beam}^{-1}$  ( $5\sigma$  noise level). The beam averaged brightness temperature of the unresolved maser spot is  $1.3 \times 10^8$  K, so that the maser gain would be a factor of  $> 10$ . Usually, this situation is seen in OH megamasers functioning as low-gain amplifiers against background continuum sources. Non-nuclear and non-disk masers have



been seen in NGC 1052 (Claussen et al. 1998) and NGC 1068 (Gallimore et al. 1996). The non-nuclear water maser known to exist in NGC 1068, located at 30 pc from the nucleus along the jet, has not been detected with VLBI, suggesting that the maser spot is resolved or not intense enough for VLBI detection. In NGC 1052 two maser spots are seen lying 0.07 pc from the presumed core along a radio jet; they show no evidence for disk structure (Claussen et al. 1998). Neither of the above cases seems to explain the maser in NGC 5793 because it exhibits different characteristics. If the water maser of NGC 5793 is emitted from the nuclear region, the large blueshift ( $\sim 245 \text{ km s}^{-1}$ ) of the maser emission implies that it traces molecular outflows moving at high speed relative to the molecular disk surrounding the nucleus. A model of a non-disk maser as described here also has problems in explaining the single-dish spectrum of the emission.

We now consider the the second possibility, namely that the masers lie in a molecular disk rotating around the nucleus of the galaxy as proposed by Hagiwara et al. (1997). Unfortunately, during the period of observations the systemic and redshifted features became weaker, and we could not measure the distribution and the velocity structure of the water masers. If we assume the presence of rotating disk, the blueshifted features could arise from the edge of the disk. The emission has been detectable and does not show any velocity drifts since its discovery in January 1996. In addition, the peak flux density is less variable than other features. Such properties are similar to the characteristics of the blue- and redshifted masers in NGC 4258 (Greenhill et al. 1995b). By contrast, the peak flux densities of features around the systemic velocity have been particularly variable. Greenhill et al. (1995a) suggested the possibility that the high-velocity features in NGC 4258 are visible for substantially longer times than the systemic ones because the emission might be self-amplified in the long gain paths along the edge of the disk. Considering these facts, the high-velocity blueshifted features may trace only a part of the disk, possibly near the tangent points. With such a supposition in mind, we propose a model (Fig. 6) for the nuclear region of NGC 5793. The location of the nucleus is presumed to lie on the midpoint of the axis connecting C1(C) to C2(E). This axis may mark the location of a two-sided jet. The blueshifted maser features are offset from this axis by  $\sim 4.5 \text{ mas}$ , or 1.0 pc. The southern side of the rotating disk, where the maser clumps lie, is approaching, while the northern side is receding. The disk orientation is nearly perpendicular to the jet. In this model, the inferred free-free absorbed source C2(E) lies within the inner radius of the disk. We estimate that the total mass enclosed within a radius of 1 pc is  $\sim 1 \times 10^7 M_{\odot}$ , assuming a rotation velocity of  $240 \text{ km s}^{-1}$  and a disk inclination of  $73^{\circ}$  (Roth 1994). The mass density is  $\sim 2 \times 10^6 M_{\odot} \text{ pc}^{-3}$ , a value that is the smallest among the megamasers observed with VLBI (Moran et al. 1999). The enclosed mass of  $\sim 10^7 M_{\odot}$  is lower approximately by a factor of 10 than that estimated from the OH absorption in the central region of  $\sim 10 \text{ pc}$  (Hagiwara et al. 2000), because we adopted a smaller radius. The sense of the disk rotation is opposite to that of the galactic

disk, which has a radius of  $\sim 1$  kpc and is observed in CO(J = 1 – 0) emission, but is the same as that of the OH absorbing gas disk, implying the existence of an independent kinematical system within the central few parsecs of the circumnuclear region.

From recent single-dish measurements made in early 2000, systemic features lying at  $V_{\text{LSR}} = 3430 \text{ km s}^{-1}$  to  $3520 \text{ km s}^{-1}$  were found to be flaring and variable in flux density (Henkel, private communication), suggesting that the features might arise against the continuum source at the nucleus along the line of sight, and that the masing cloud is amplifying the background continuum source.

## 5. SUMMARY

We have observed the water megamasers and continuum emission in the nuclear region of the Seyfert 2 galaxy NGC 5793 with the VLBA. Because of the faintness of the maser intensities, only the blueshifted emission could be imaged. This emission, which is located 3.6 pc southwest of the radio continuum source, is observed to consist of two clusters with a separation of 0.7 mas (0.16 pc). No compact continuum emission was detected near to the maser spot. The detected water maser could be a part of a maser disk as in the case of NGC 4258. We propose a model in which the masers lie on the southern edge (approaching side) of a rotating molecular gas disk whose orientation is nearly perpendicular to the jet. Assuming the location of the nucleus at a midpoint between C1 and C2(E) one can estimate a binding mass on the order of  $10^7 M_{\odot}$ . Alternatively, the masers could result from the amplification of a radio jet by foreground circumnuclear gas. The highly blueshifted velocity of the maser features might mean that the masing cloud traces outflowing gas surrounding an active nucleus.

The compact continuum source, C2(E) appears to have an inverted spectrum between 1.7 and 5.0 GHz, assuming no intrinsic variability, and the spectral turnover might be due to synchrotron self-absorption caused by a shock in the jet owing to collision with the dense gas, or a free-free absorbing screen in a part of an ionized torus/disk.

Further VLBI observations of the water masers and continuum emission are crucial to clarify the dynamical structures of the maser emission in relation to the active nucleus. The systemic and redshifted velocity features flared in early 2000 and additional VLBA observations, following up our present result, are already underway.

We are grateful to Drs. R. Porcas, E. Ros, C. Henkel, and A. Roy for their helpful comments and suggestions. We also appreciate J. Conway and Y. Pihlström for providing us the 1.4 GHz image. YH appreciates the efforts of P. Hall, E. Troup, and other staff members at Parkes for their assistance in the observations and data analysis. Part of the

VLBA observations appearing in this paper were conducted while PJD was an NRAO staff member. This research has made use of NASA's Astrophysics Data System Abstract Service.

## REFERENCES

- Baan, W. A., Salzer, J. J., & LeWinter, R. D. 1998, *ApJ*, 509, 633
- Braatz, J. A., Wilson, A. S., & Henkel, C. 1997, *ApJS*, 110, 321
- Carilli, C. L., & Holdaway, M. A. 1999, *Radio Science*, 34, 817
- Claussen, M. J., Diamond, P. J., Braatz, J. A., Wilson, A. S., & Henkel, C. 1998, *ApJ*, 500, L129.
- Falcke, H., Henkel, Chr., Peck, A. B., Hagiwara, Y., Prieto, M. A., & Gallimore, J. F. 2000, *A&A*, 358, L17
- Gallimore, J. F., Baum, S. A., & O’Dea, C. P. 1996, *ApJ*, 464, 198
- Gardner, F. F., & Whiteoak, J. B. 1986, *MNRAS*, 221, 537
- Gardner, F. F., Whiteoak, J. B., Norris, R. P., & Diamond, P. J. 1992, *MNRAS*, 258, 296
- Greenhill, L. J., Jiang, D. R., Moran, J. M., Reid, M. J., Lo, K.-Y., & Claussen, M. J. 1995a *ApJ*, 440, 619
- Greenhill, L. J., Henkel, C., Becker, R., Wilson, T. L., & Wouterloot, J. G. A. 1995b, *A&A*, 304, 21
- Greenhill, L. J., Gwinn, C. R., Antonucci, R., & Barvanis, R. 1996, *ApJ*, 472, L21
- Greenhill, L. J., & Gwinn, C. R. 1997, *Ap&SS*, 248, 261
- Greenhill, L. J., Moran, J. M., & Herrnstein, J. R. 1997, *ApJ*, 481, L23
- Greenhill, L. J. 2000, in the Proceedings of the 5th EVN Symposium. eds. Conway, J. E., Polatidis, A. G., Booth, R. S. & Pihlström, Y. M. (Onsala Space Observatory, Sweden), p101
- Hagiwara, Y., Kohno, K., Nakai, N., & Kawabe, R. 1997, *PASJ*, 49, 171
- Hagiwara, Y. 1998, Ph.D Thesis, The Graduate University for Advanced Studies
- Hagiwara, Y., Diamond, P. J., Nakai, N., & Kawabe, R. 2000, *A&A*, 360, 49.
- Herrnstein, J. R., Greenhill, L. J., Moran, J. M., Diamond, P. J., Inoue, M., Nakai, N., & Miyoshi, M. 1998, *ApJ*, 497, 69

- Ishihara, Y., Nakai, N., Iyomoto, N., Makishima, K., Diamond, P., & Hall, P. 2001, PASJ, 53, 215
- Kellermann, K. I., & Pauliny-Toth, I. I. K. 1969, ApJ, 155, 71
- Miyoshi, M., Moran, J., Herrnstein, J., Greenhill, L., Nakai, N., Diamond, P., & Inoue, M. 1995, Nature, 373, 127
- Moran, J. M., Greenhill, L. J., & Herrnstein, J. R. 1999, J. Astrophys. Astron., 20, 165
- Nakai, N., Inoue, M., Miyazawa, K., Miyoshi, M., & Hall, P. 1995, PASJ, 47, 771
- Nakai, N., Inoue, M., Hagiwara, Y., Miyoshi, M., & Diamond, P. J. 1998, in Radio Emission from Galactic and Extragalactic Compact Sources., ed. J. A. Zensus, G.B. Taylor, & J. M. Wrobel (San Francisco: ASP), 237
- Palumbo, G. G. C., Tanzella-Nitti, G., & Vettolani, G. 1983, in Catalogue of radial velocities of galaxies., (New York: Gordon and Breach Science Publishers)
- Pihlström, Y. M., Conway, J. E., Booth, R. S., Diamond, P. J., & Koribalski, B. S. 2000, A&A, 357, 7
- Roth, J. 1994, AJ, 108, 862

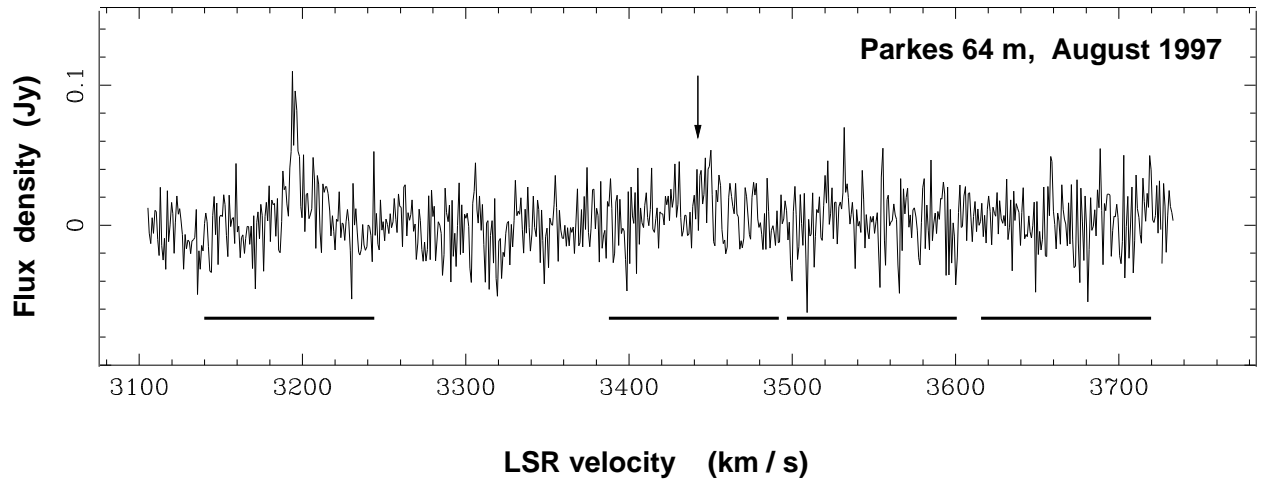


Fig. 1.— Spectrum of the H<sub>2</sub>O maser towards the center of NGC 5793, observed with the Parkes radio telescope of the CSIRO. The spectrum is averaged over three days from 18-20 August 1997. Accuracy of the flux density is about 10 %. A downward arrow indicates the adopted systemic velocity of the galaxy,  $V_{\text{LSR}} = 3442 \text{ km s}^{-1}$ . Solid bars indicate the velocity ranges covered by four IFs which we observed with the VLBA in May 1998.

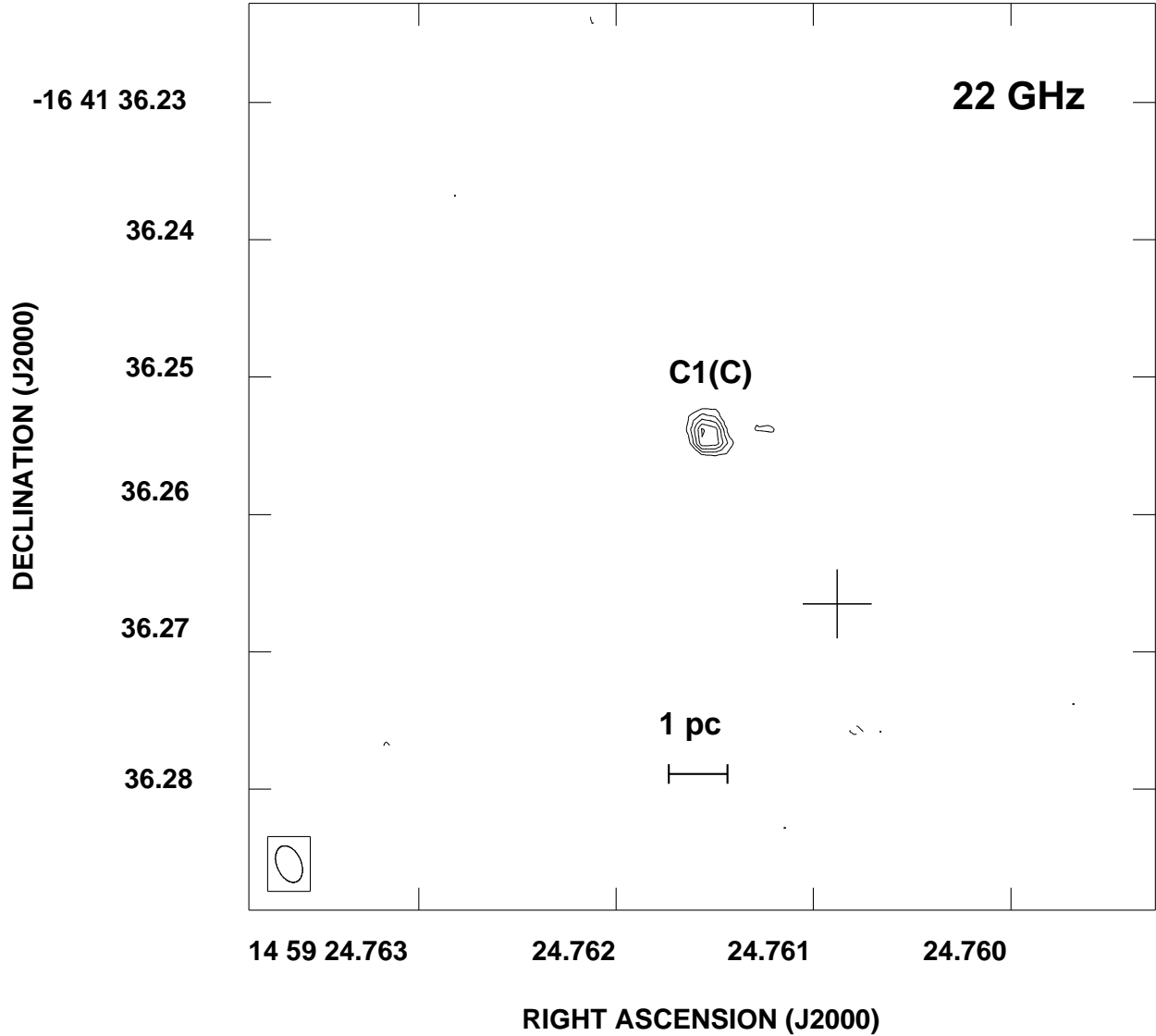


Fig. 2.— Radio continuum image at 22 GHz with the VLBA. The levels of contours are  $-3, 3, 4, 5, 6, 7\sigma$  ( $1\sigma = 1.3 \text{ mJy beam}^{-1}$ ). The peak flux density is  $9.2 \text{ mJy beam}^{-1}$ . The synthesized beam of  $2.8 \times 1.8 \text{ mas}$  at  $\text{P.A.} = 23^\circ$  is plotted in the left-hand corner. The cross marks the Gaussian-fitted center of a maser feature at  $V_{\text{LSR}} = 3194 \text{ km s}^{-1}$ . The relative alignment of the maser and continuum is accurate to  $0.22 \text{ mas}$ .

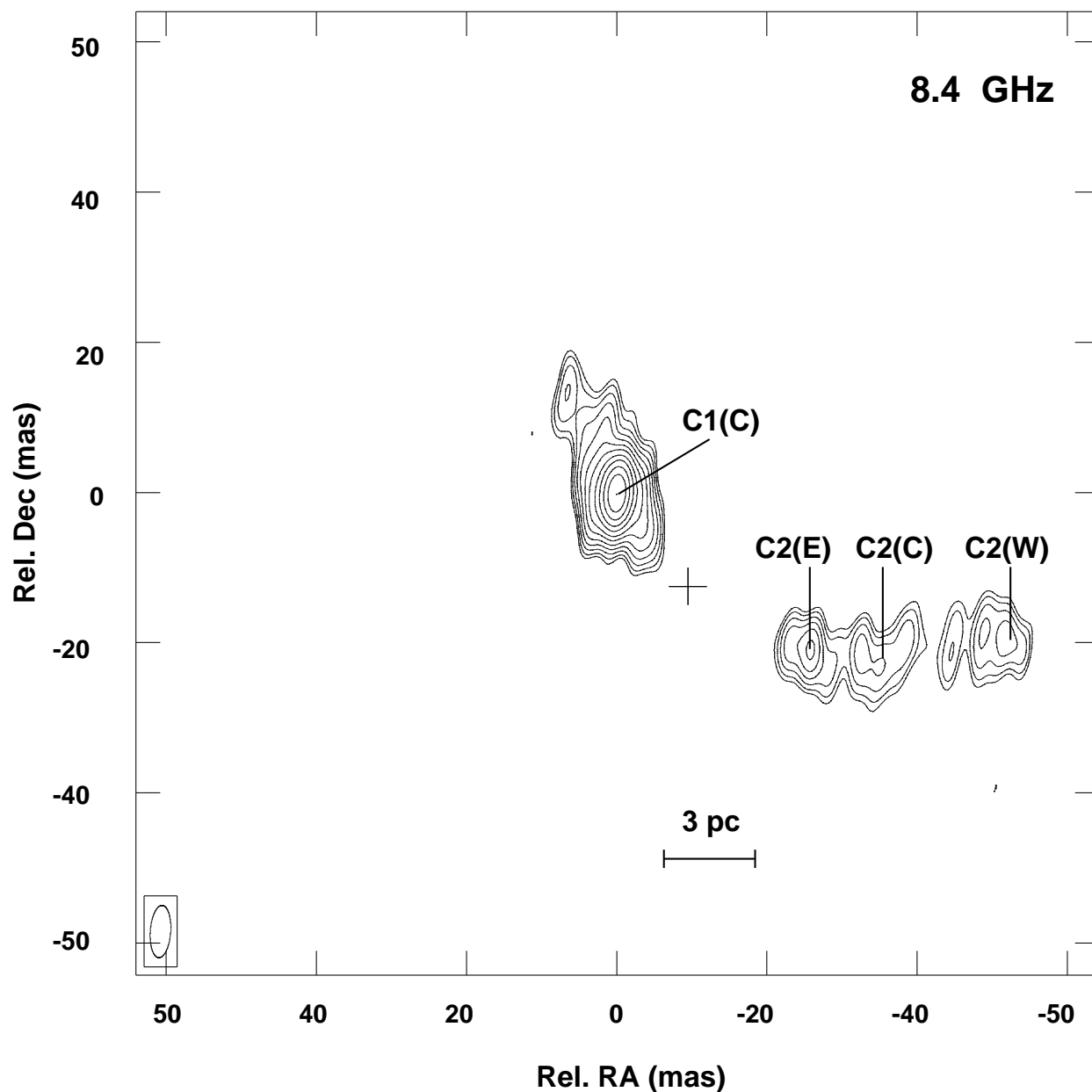


Fig. 3.— 8.4 GHz radio continuum image of the nuclear region made with the VLBA. The contour levels are  $-2.7, 2.7, 3.7, 5.2, 7.2, 10, 14, 19, 27, 37, 52, 72,$  and  $100\%$  of the peak flux density of  $51.1 \text{ mJy beam}^{-1}$ . The synthesized beam of  $7.0 \times 2.7 \text{ mas}$  at  $\text{P.A.} = -4.7^\circ$  is shown in the left-hand corner. The position of the maser feature at  $V_{\text{LSR}} = 3194 \text{ km s}^{-1}$  is marked by a cross. The center position  $(0, 0)$  in the map coincides with that of the 22 GHz continuum peak in Fig. 2. The relative accuracy of the 8.4 GHz continuum and 22 GHz maser positions is  $\sim 0.2 \text{ mas}$ .



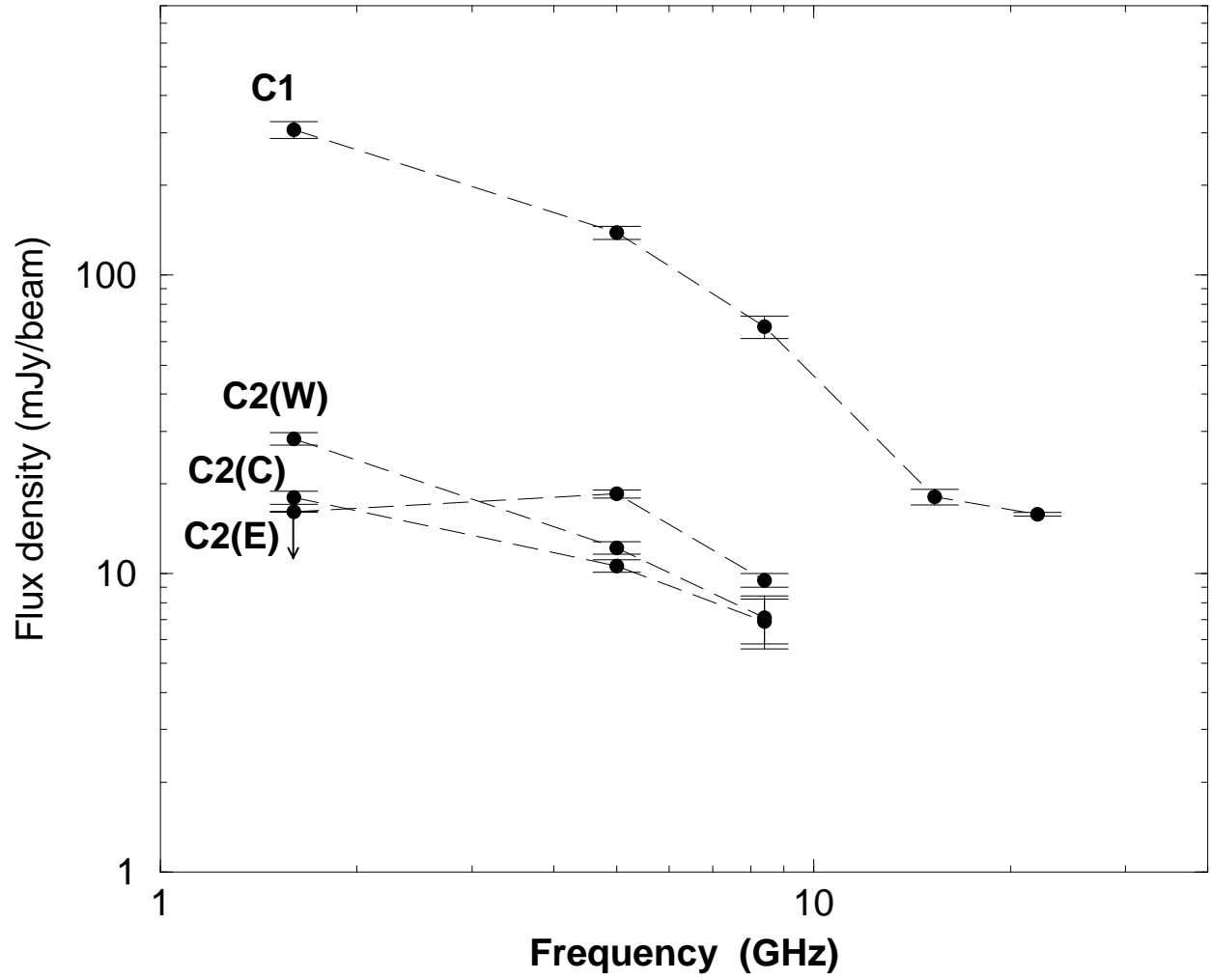


Fig. 4.— Continuum spectra of the four compact components C1(C), C2(E), C2(C), and C2(W) at 1.7, 5.0, 8.4, 15 and 22 GHz. The flux density of C2(E) at 1.7 GHz is an upper limit.

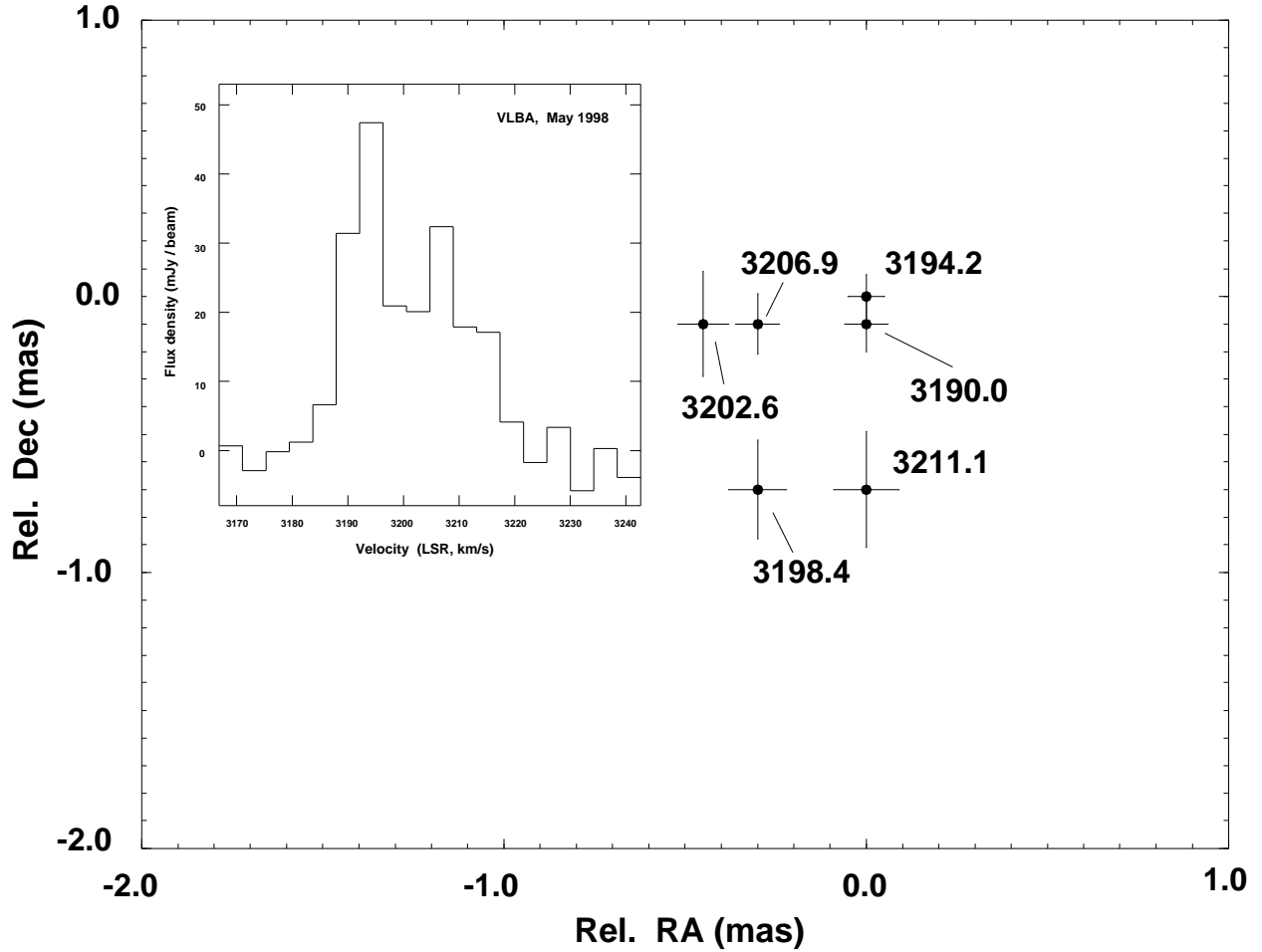


Fig. 5.— Distributions of water maser emission. The position of each component was estimated by 2-D Gaussian-model fitting, and error bars indicate total positional uncertainties of  $1\sigma$ . The point (0, 0) is referred to position of the crosses in Fig. 2 and Fig. 3. The maser spots are labelled by their velocities in  $\text{km s}^{-1}$ . The inset shows the VLBA spectrum of the blueshifted maser emission. Five spectral channels were averaged to  $4.2 \text{ km s}^{-1}$  (channel spacing before averaging is  $0.84 \text{ km s}^{-1}$ ). Accuracy of the flux density scale is typically 5 %.

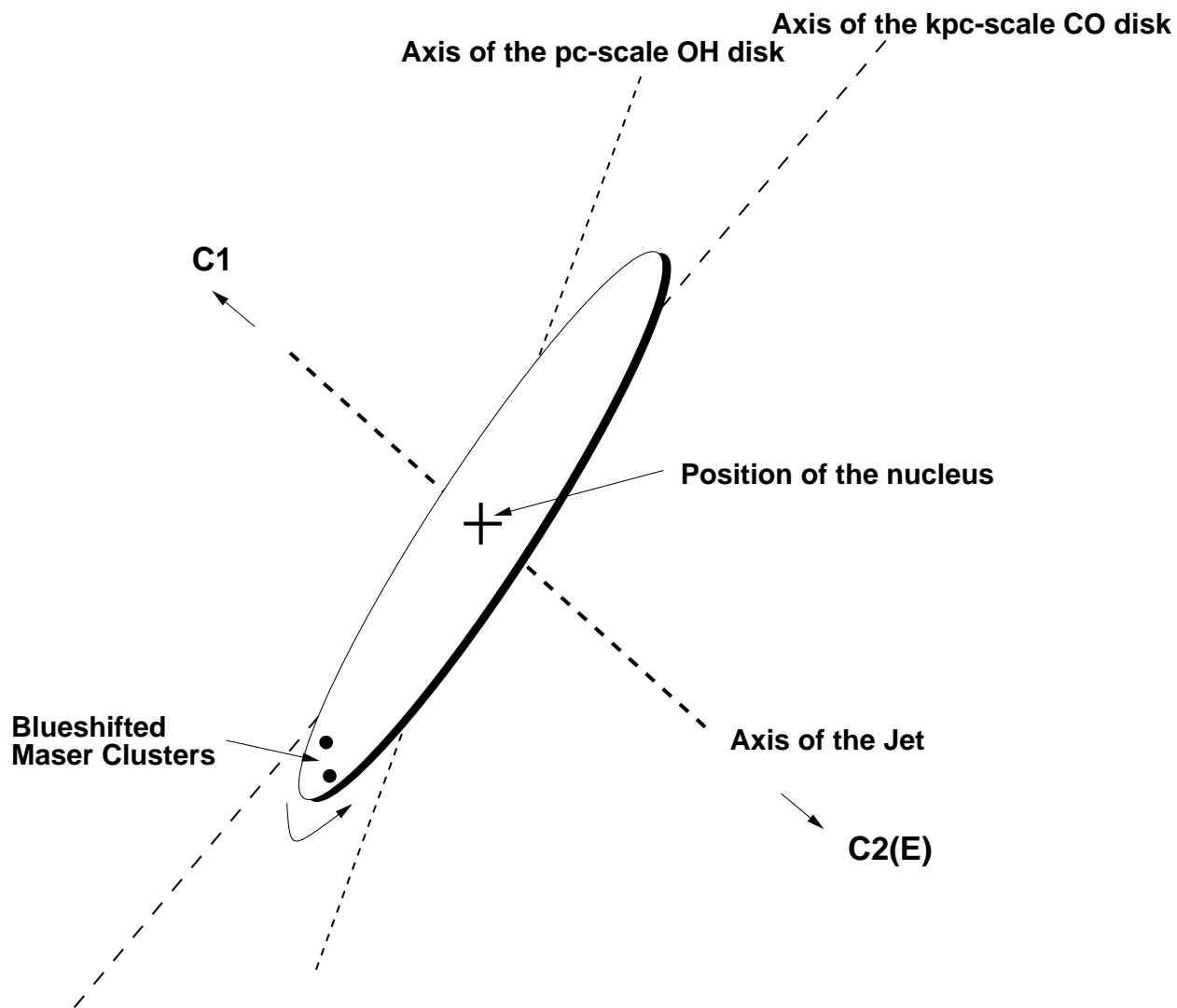


Fig. 6.— Schematic view of the nuclear region of NGC 5793. The position of the nucleus is assumed to lie at the midpoint on the line joining C1 and C2(E). The blueshifted maser clusters are located on the approaching side of a postulated edge-on rotating disk. The P.A. of the disk lying nearly perpendicular to the jet is well aligned with the kiloparsec-scale disk observed in CO emission, and the pc-scale disk imaged in OH absorption (Hagiwara et al. 2000). An arrow denotes the sense of the rotation of the maser disk. The sense is the same as that of the OH disk, but reversed when compared to that of the CO disk.

Table 1. FLUX DENSITIES OF MAJOR COMPONENTS

Frequency Band (GHz)	Component Flux Densities (mJy beam <sup>-1</sup> )				Epoch	Reference
	C1(C)	C2(E)	C2(C)	C2(W)		
1.4 ...	304	16.3	15.6	23.1	Dec. 96	a
1.7 ...	308	<16.1 <sup>d</sup>	18.0	28.3	Nov. 96	b
	274	< 15.2 <sup>d</sup>	13.9	14.7	Oct. 99	c
5.0 ...	139	18.5	10.6	12.2	Oct. 97	b
8.4 ...	64.5	9.42	6.73	7.31	Oct. 99	c
15 ...	16.4	...	...	...	Oct. 99	c
22 ...	16.3	...	...	...	May 98	c

<sup>a</sup>Y. Pihlström, private communication

<sup>b</sup>Hagiwara et al. 2000

<sup>c</sup>This paper

<sup>d</sup>An upper limit value

Note. — Flux uncertainties assume 5 percent calibration uncertainty added. All the flux densities are estimated with the synthesized beam at 1.7 GHz (12.4 × 4.4 mas).

Table 2. SPECTRAL INDICES OF MAJOR COMPONENTS

Frequency Range (GHz)	Component Spectra, $\alpha$ ( $S_\nu \propto \nu^\alpha$ )			
	C1(C)	C2(E)	C2(C)	C2(W)
1.7 <sup>a</sup> – 5.0 ...	-0.70	0.13	-0.46	-0.72
5.0 – 8.4 ...	-1.5	-1.3	-0.88	-0.99
8.4 – 15 ...	-2.3	...	...	...
15 – 22 ...	-0.017	...	...	...

<sup>a</sup>Data from Nov. 1996